Computational study of the intercalation of NO_2 between bilayer $MoTe_2$

Maciej J. Szary*

Institute of Physics, Poznan University of Technology, ul. Piotrowo 3, 61-138 Poznan, Poland

E-mail: maciej.szary@put.poznan.pl

Abstract

Transition-metal dichalcogenide (TMD) layers have been a subject of widespread interest as chemical sensors with their sensitivity selectively enhanced depending on the number of layers. The effect has been linked to possible intercalation of species such as nitrogen dioxide (NO_2). However, whether intercalation helps or even occurs remains speculative. Hence, this work investigates, employing density functional theory (DFT) calculations, the intercalation of NO_2 between bilayers of molybdenum ditelluride ($MoTe_2$), its energy, and the impact on charge transfer. The effects are confronted with the intercalation of nitrogen molecules (N_2) and the equivalent adsorption of both species. The results show that the intercalation of NO_2 can be energetically favorable for < 0.4, 1.5–3.0, and > 4.0 molecules/nm^2 and that at low coverage, the molecule-sheet interactions are too weak to facilitate sufficient interlayer expansion, and thus the molecules dissociate. The dissociation and non-dissociative intercalation of NO_2 enhance the per molecule charge transfer by 1110% and 256%, respectively, relative to adsorption. Hence, in all favorable cases, the intercalation should significantly enhance the response of the system. Furthermore, the results suggest that the evacuation of NO_2 should be feasible, allowing $MoTe_2$ recovery. In contrast, N_2 intercalation is unfavorable, illustrating the selectivity of the process.

Keywords

nitrogen dioxide, molybdenum ditelluride, surface interactions, intercalation, density functional theory

1 Introduction

Motivated by the novel properties and emerging application possibilities, two-dimensional materials (2DM) have been extensively investigated, with discoveries surging in recent years[1–6]. Among them, transition-metal dichalcogenide (TMD) layers have gained particular interest because of their unique properties, facilitated by different elements and stacking polytypes. Each TMD sheet consists of a transition-metal layer (Mo, W, etc.) stacked between two chalcogen layers (S, Se, or Te). Atoms within the sheet form strong-ionic/covalent bonds, with transition metals adopting trigonal-prismatic (2H) or octahedral (1T) coordination. In contrast, the interactions between individual three-layer sheets are limited to van der Waals (vdW) attraction, which has allowed micromechanical exfoliation and intercalation of foreign species into the vdW gaps of the TMD sheets.

The effect has been extensively explored for ions (Li^+, Na^+, etc.), as TMDs are a promising platform for electrodes in rechargeable batteries[7–14]. Intercalation has also been investigated for molecules, showing that it can improve the diffusion kinetics of ions[15–18], enhance

hydrogen evolution reactions (HER)[19–21], and impact the lubricity[22,23]. However, relatively little is known about the effects of intercalation on the sensing performance of multilayer TMDs, even though they are currently a subject of widespread interest as chemical sensors[2,24–27].

Effective sensors require a good balance between the adsorption energy (E_{ads}) and the charge transfer (δQ) resulting from the molecule-sheet interaction. This is because desorption rates are critically dependent on E_{ads}. Thus, low values are needed for a fast response of the sensor to rapid changes in the concentration of the monitored gas. However, the interactions must also facilitate a sufficiently large δQ to affect the conductivity and/or photoluminescence of the sensing layer, allowing detection. As a consequence, TMDs have been considered a model material for chemical sensors as interactions on their surfaces are mostly limited to physisorption, and their excellent surface-to-volume ratio makes the accumulative impact on their carrier concentration relatively large. This has led TMDs such as molybdenum disulfide (MoS_2) and molybdenum ditelluride ($MoTe_2$) to be particularly sensitive to molecules of nitrogen dioxide (NO_2)[24,28–30] and ammonia (NH_3)[30–33]. Interestingly, the sensitivity has been reported selectively enhanced depending on the number of layers[34]. The response of the five-layer MoS_2 was found to be several times higher than the one measured for the two-layer structure, despite the low impact on the electronics of MoS_2 for two or more layers[35]. On the other hand, the effect was significantly lower for NH_3[34].

The findings are consistent with intercalation since it should introduce more surface area, and as the intercalation energy (E_{int}) is a sum of the exothermic molecule-sheet interactions and the endothermic interlayer expansion, the effect should be specie-dependent. However, the results could also correlate with other effects, e.g., adsorption at the edges. Hence, the impact of intercalation on the sensing performance of multilayer TMDs, or even whether it occurs, remains uncertain. The effect was discussed briefly by Bermudez[24], where it was found, employing density functional (DFT) computations for a (2×2) supercell of a bilayer 2H-MoS_2, that δQ for intercalated NO_2 is approximately twice the transfer facilitated by adsorption. This has suggested that intercalation could indeed improve the response of a few-layer MoS_2 to NO_2. However, since the effect was not the main focus of the study, only one model case had been considered, and it has resulted in the intercalation being unfavorable.

Nevertheless, the stability of processes such as adsorption and intercalation can notably depend on the concentration of species[36–39]. Therefore, intercalation of NO_2 could still be possible. Furthermore, it was argued that other species that adsorb more strongly or require less expansion should be more favorable for intercalation[24]. Likewise, TMDs with weaker binding between sheets or larger vdW gaps (e.g., $MoSe_2$ and $MoTe_2$[40–42]) should also allow for more effective intercalation. Thus, the effects may differ between TMDs.

Consequently, this work investigates, employing DFT calculations, the intercalation of NO_2 between bilayers of $MoTe_2$, its energy E_{int} and the impact on δQ. The effects are confronted with the intercalation of N_2 and the equivalent adsorption of both species. $MoTe_2$ has been selected in favor of MoS_2 for several reasons. Both have a high sensitivity to NO_2. However, $MoTe_2$ has a considerably larger vdW gap and weaker binding between its layers. Furthermore, because of its smaller band gap, ultraviolet (UV) radiation can efficiently generate electron-hole pairs in the sheets[2], which in turn facilitates recombination with electrons trapped in adsorbed molecules[43,44]. Thus, UV light can greatly enhance the sensitivity and recovery rate of NO_2 gas sensors based on $MoTe_2$[2,32], which should be particularly relevant for multilayer systems, as intercalation may slow recovery.

2 Computational Details

The computational results presented in this report employed a plane-wave/pseudopotential (PW/PP) approach of DFT as implemented in the Quantum ESPRESSO package[45–47]. The schematics of the atomic structures (Figures 1, 3, 4, and 8) were created using the XCrySDen visualization program[48]. Since NO_2 is paramagnetic, all calculations were spin-unrestricted. The Perder-Burke-Ernzerhof (PBE) functional was used[49,50] with the Rappe-Rabe-Kaxiras-Joannopoulos ultrasoft pseudopotentials[51,52], and cut-off energies for the plane wave and the electron density of 56 and 480 Ry, respectively. The adopted pseudopotentials have included scalar-relativistic and nonlinear core corrections. Grimme's DFT-D3 method has been used to treat the vdW contributions to the total energy[53].

Ab initio molecular dynamics (AIMD) simulations were based on the Born-Oppenheimer approximation. Total energy and gradients were obtained from DFT calculations, while the motions of the nuclei were

treated using the velocity Verlet algorithm. The timestep was set at 20 au (0.9676 fs), which is less than one-tenth of the maximum vibration frequency period for NO_2 + $MoTe_2$, i.e., the antisymmetric N-O stretch ($\approx$ 20 fs). The target temperature was set at 300 K.

The charge transfers were calculated from the Löwdin population analysis of pseudoelectron density (that is, only valence electron density). Therefore, the core electrons were not included, and thus only the net changes on the valence shells were investigated.

Monolayer and bilayer $MoTe_2$ were modeled using 2D periodic slabs. The investigation included 3×3, 4×4, and 5×5 cells, which follows the methodology used in other studies on the adsorption of molecules on the surfaces of TMDs[25–27]. The cell height was set at 32 Å to minimize artificial interactions between the neighboring systems. The positions of all atoms in the atomic structure were relaxed in total energy optimization with the convergence threshold of $< 10^{-4}$ Ry/au adopted for the forces.

3 Results and discussion

3.1 Modeling intercalated 2H-$MoTe_2$. Intercalation between sheets of layered materials entails an endothermic interlayer expansion and deformation (E_{endo}), coupled with an exothermic molecule-sheet interaction (E_{exo}). Therefore, the process often has a notable impact on the total energy of the system ($E_{\text{int}} = E_{\text{endo}} + E_{\text{exo}}$), making the intercalation energy one of the main factors in intercalation investigations[54–56]. Furthermore, as E_{int} represents the change to the total energy, it can be quantified as the difference between the energy of intercalated 2DM [E(mol.+2DM)] and the free molecules [E(mol.)] and the sheets [E(2DM)] employing the formula:

$$\begin{aligned} E_{\text{int}} &= E_{\text{endo}} + E_{\text{exo}} \\ &\equiv E(\text{mol.+2DM}) - E(\text{mol.}) - E(\text{2DM}). \end{aligned} \tag{1}$$

Thus, if E_{int} is negative, the intercalation is energetically favorable, while when it is positive, the process is unfavorable and leads to a destabilization of the system.

As a consequence, species that require less expansion or interact strongly with 2MD are typically more favorable for intercalation. As such, NO_2, being a free radical, is likely to favor relatively strong physisorption even on chemically inert surfaces of $MoTe_2$. Hence, to expand the context of the investigation and allow a comparison of the NO_2 results with a case that should strongly disfavor intercalation, N_2 has been included in the study.

The interaction between the sheets of $MoTe_2$ and the intercalated molecules will likely be limited to physisorption. Thus, rather than having one well-defined global energy minimum, the intercalation is likely to result in a number of different configurations characterized by similar E_{int} and low energy barriers separating them. As such, this investigation adopts the AIMD approach to identify the most stable intercalation configurations. The approach employs surface diffusion of molecules to probe different binding sites and configurations without bias inherent in predefined geometries. The resulting time evolution of a system can be subsequently analyzed, and based on the adopted criteria, local minima can be selected, and their structures used in the following structural optimization.

The AIMD calculations have adopted the 3×3 supercell of 2H-$MoTe_2$ (see Figures 1a and 1d), with one molecule per supercell. The initial positions of NO_2 and N_2 are shown in Figures 1b and 1c, respectively. The molecules have been aligned "flat" (parallel to the surface) and placed between two parallel hexagonal rings of the upper and lower layers (the hexagon has been highlighted in yellow in Figure 1d).

Variations in total energy during AIMD of NO_2+2H-$MoTe_2$ and N_2+2H-$MoTe_2$ are shown in Figures 2a and 2b, respectively. The time evolution of the molecular dynamics of both systems has been presented between 0.2 and 2.2 ps. In both cases, four characteristic configurations have been selected based on three criteria.

1. All configurations had to be a local energy minimum.
2. They had to be distinctly different from each other (probing different binding sites and/or having a unique orientation of the molecule).
3. They had to have notable energy barriers between subsequent configurations and/or different total energies (minimizing the risk of relaxing into equivalent configurations).

3.2 The optimized configurations of the intercalated 2H-$MoTe_2$. Table 1 summarizes the relevant parameters of the optimized intercalation configurations and complementary adsorption on monolayer 1H-$MoTe_2$ labeled "ads". For both molecules, the 1st

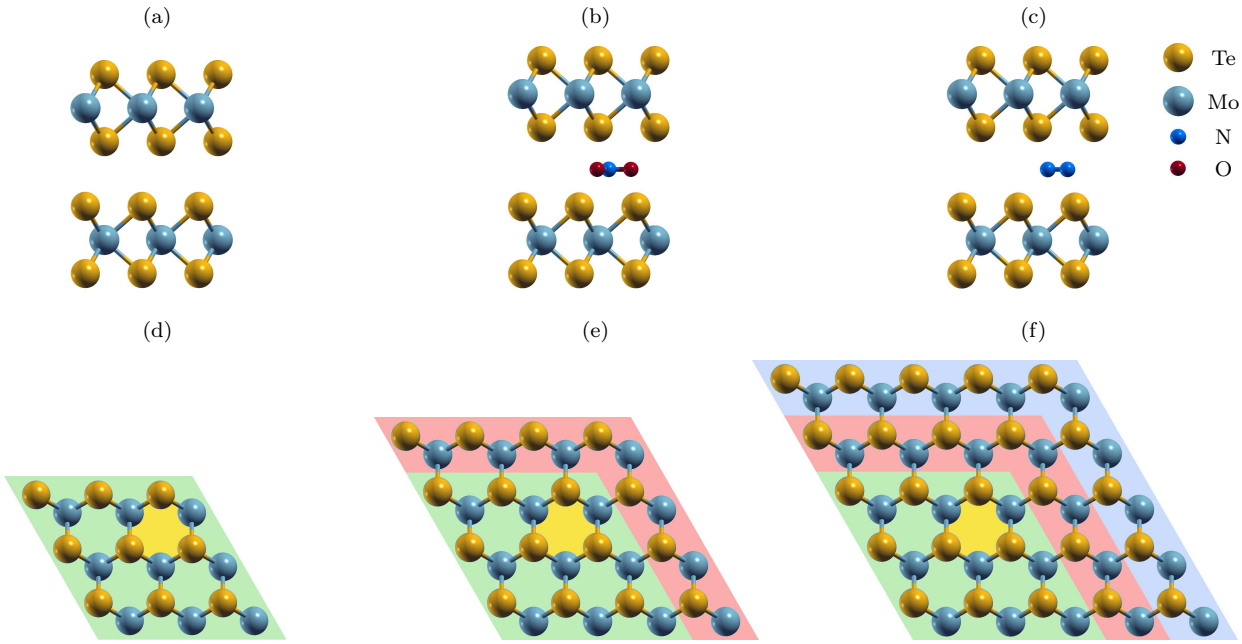

Figure 1: Schematics of atomic structures of $MoTe_2$ (a), initial AMID configurations for NO_2+2H-$MoTe_2$ (b), and N_2+2H-$MoTe_2$ (c). Top views of 3×3 (d), 4×4 (e) and 5×5 (f) cells of $MoTe_2$. Green, red, and blue highlights indicate the 3×3 cell, and the expansions into 4×4 and 5×5, respectively. Yellow highlight indicates the initial placement of a molecule in AMID.

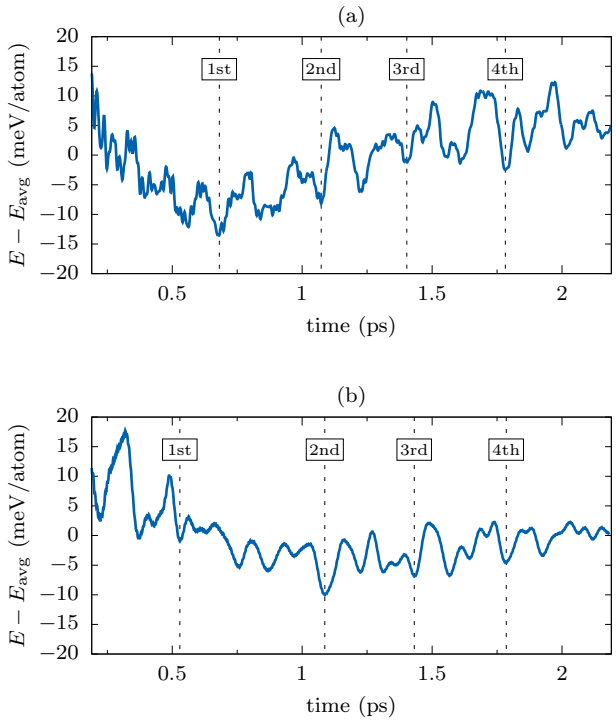

Figure 2: Variation of total energy during AMID simulation of NO_2+2H-$MoTe_2$ (a), and N_2+2H-$MoTe_2$ (b).

configuration results in the lowest total-energy structures, which following Equation 1 translates to the lowest E_{int}. The schematic representation of those structures is shown in Figure 3. In the case of NO_2+2H-$MoTe_2$ (Figure 3a and 3c), the molecule favors a vertical alignment with O atoms facing one of the sheets while N facing the other. The molecule also seems to relax at the bridge position between Mo and Te atoms, which is similar to the reported adsorption of NO_2 on 1H-MoS_2 [24]. The process has a limited impact on the atomic structure of the sheet and the molecule, but it has a notable effect on the vdW gap. Before intercalation, the vertical separation between the interfacing

Table 1: Adsorption and intercalation of NO_2 and N_2

	conf.	E_{int} [a]	E_{exo} [b]	E_{endo} [c]	δQ [d]	$h_{Te\text{-}Te}$ [e]
NO_2+2H-$MoTe_2$	1st	1.265	−0.341	1.606	0.425	5.659
	2nd	1.399	−0.473	1.871	0.319	6.165
	3rd	1.531	−0.440	1.972	0.300	6.500
	4th	1.708	−0.376	2.084	0.231	7.038
NO_2+1H-$MoTe_2$	ads	–	−0.231	–	0.166	–
N_2+2H-$MoTe_2$	1st	1.703	−0.008	1.711	0.066	5.948
	2nd	1.704	−0.032	1.736	0.061	6.022
	3rd	1.706	−0.011	1.716	0.067	5.902
	4th	1.705	−0.027	1.732	0.060	6.009
N_2+1H-$MoTe_2$	ads	–	−0.099	–	0.009	–

[a] E_{int} is the intercalation energy (eq 1, eV), [b] E_{exo} is the energy of the exothermic molecule-sheet interaction (eq 2 and 3, given in eV/nm^2), [c] E_{exo} is the energy of the endothermic layer expansion and deformation (eq 4, given in eV/nm^2), [d] δQ is the electron transfer from $MoTe_2$ to the molecule (given in $-e$), [e] $h_{Te\text{-}Te}$ is the vertical distance between the interfacing layers of Te (given in Å).

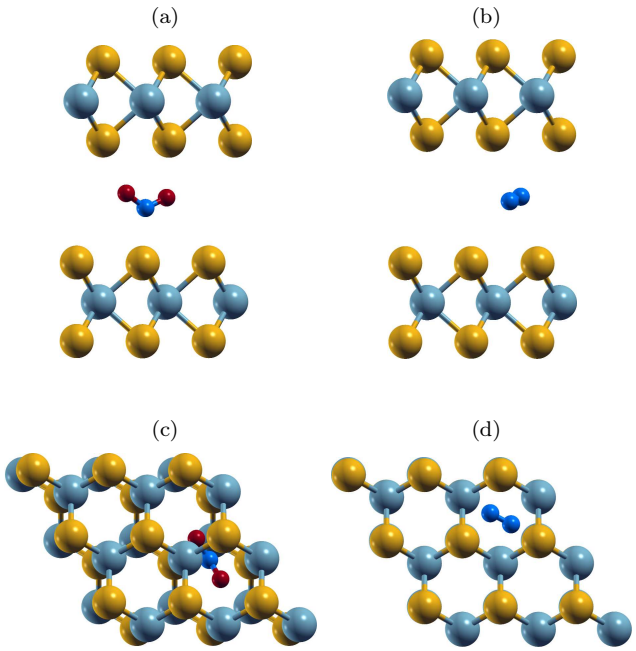

Figure 3: Schematics of atomic structures of the lowest energy configuration of NO_2+2H-$MoTe_2$ (a,c), and N_2+2H-$MoTe_2$ (b,d).

Te atoms of the upper and lower sheets of 2H-$MoTe_2$ ($h_{\text{Te-Te}}$) is 3.492 Å. However, after NO_2 intercalation, its value increases to 5.659 Å. The effect can be even higher for the other configurations (see Table 1), despite them favoring the same type of vertical orientation. The process is shown to also affect the stacking alignment of the sheets, which may have an impact effect on the stability of the system. On the other hand, in the case of N_2+2H-$MoTe_2$ (Figures 3b and 3d), the molecule favors a horizontal alignment centered between two parallel hexagonal rings of the upper and lower sheets of $MoTe_2$. The intercalation has a low impact on the structure of the sheets and N_2 while having a notable effect on the vdW gap of 2H-$MoTe_2$. However, unlike the NO_2 case, the values of $h_{\text{Te-Te}}$ show little variation between the configurations, and none of them has affected the stacking of the sheets.

3.3 The charge transfer in the intercalated 2H-$MoTe_2$. The impact of intercalation on the atomic structure of the system has a significant effect on charge transfer and stability. In the case of transfer, notable differences can be seen between (i) configurations of NO_2+2H-$MoTe_2$, (ii) NO_2+2H-$MoTe_2$, and N_2+2H-$MoTe_2$, as well as (iii) intercalation and adsorption. Table 1 shows the values of the charge transfer per molecule. However, for ease of analysis, the transfers per atom are illustrated by the histograms given in Figures 4a and 4b. In both cases, the values of δQ were calculated as the net charge changes in the molecules, i.e., the sum of per orbital population differences in the atoms comprising NO_2 or N_2 when free and after intercalation or adsorption.

The results for NO_2 show that in all cases the molecule-sheet interaction gives rise to an electron transfer, resulting in the molecule accumulating a negative charge. The values are high, but they differ notably between the structures (see Figure 4a). The 1st intercalation configuration has the highest value of δQ, coinciding with the smallest $h_{\text{Te-Te}}$ and the lowest E_{int} (see Table 1). The remaining configurations have lower transfers coupled with wider gaps and higher energies, illustrating the direct correlation between charge transfer and interaction distances. This is further demonstrated by results for NO_2+1H-$MoTe_2$. The adsorption case employed the atomic structure of the 1st intercalation configuration, but without the upper sheet of $MoTe_2$ and with a subsequent structure optimization. The resulting structure gives rise to the lowest value of δQ. Of course, it is in part due to NO_2 interacting with only one sheet. Figures 4c and 4d show the difference in electron density, given by $\delta n = n(\text{mol.}+\text{1H/2H-MoTe}_2) - n(\text{mol.}) - n(\text{1H/2H-MoTe}_2)$, where n is the total density of pseudoelectrons, It is evident that NO_2 accumulates more electronic charge while interacting with both upper and lower sheets. However, when inspecting the total value of δQ (Figure 4a), it can be seen that its value for NO_2+1H-$MoTe_2$ is less than half of the transfer for the 1st configuration of NO_2+2H-$MoTe_2$. Thus, the difference must result from the increased molecule-sheet separation occurring during NO_2+1H-$MoTe_2$ optimization.

Similar trends can also be ascertained from the results for N_2. The molecule accumulates electronic charge due to the molecule-sheet interaction, but the effect is significantly less pronounced compared to NO_2 (compare Figures 4a with 4b and 4c,d with 4e,f). Still, since intercalation reduces the distance between N_2 and $MoTe_2$ relative to adsorption, N_2+2H-$MoTe_2$ facilitates higher transfers than N_2+1H-$MoTe_2$. Furthermore, because the intercalated configurations share approximately equal vdW gap, they also have virtually identical charge-transfer values. The results suggest that the intercalation may generally favor higher charge transfer relative to adsorption, which could prove beneficial for molecular sensing, depending on its impact on system stability and sensor response time.

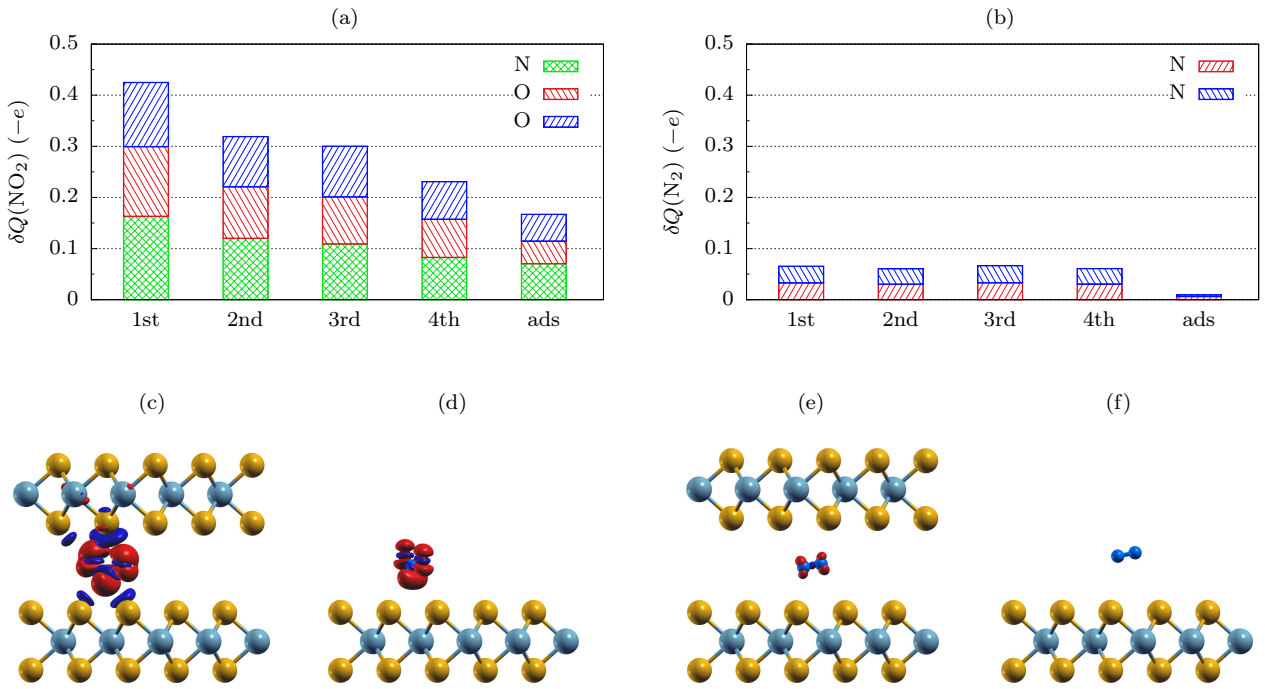

Figure 4: The charge differences in atoms of NO_2 (a) and N_2 (b) upon intercalation and adsorption. The charge density contours for the 1st configuration of NO_2+2H-$MoTe_2$ (c), NO_2+1H-$MoTe_2$ (d), N_2+2H-$MoTe_2$ (e), and N_2+1H-$MoTe_2$ (f). Isosurface values of 0.001 e/Bohr^3.

3.4 The intercalation energy. The results show that the intercalation energy differs for the molecules of NO_2 and N_2. It also varies between configurations of NO_2+2H-$MoTe_2$ ranging between 1.265 and 1.708 eV/nm^2. On the other hand, all configurations of N_2+2H-$MoTe_2$ facilitate E_{int} of $\approx$ 1.7 eV/nm^2 (see Table 1). Thus, the process is more favorable for NO_2 than N_2, but both destabilize the system. Of course, those are only some of many intercalation configurations, so it remains to be seen whether the process is universally unfavorable or only in some cases. However, before continuing the investigation, it is necessary to ascertain what makes the intercalation of NO_2 and N_2 unfavorable. This will elucidate the problem and help determine appropriate changes. Consequently, the intercalation needs to be inspected in more detail, especially its exothermic and endothermic components and how the molecule-sheet interactions differ when the molecules are intercalated and adsorbed on the surface of $MoTe_2$.

The values of E_{exo} and E_{endo} have been given in Table 1, but for ease of analysis, they have also been illustrated in the histograms shown in Figures 5a and 5b. In the case of intercalation, E_{exo} has been calculated as the difference between the total energy of the intercalated system [E(mol.+2H)], the energy of the free molecule [E(mol.)], and the energy of the interlayer-expanded 2H-$MoTe_2$ [E(IE-2H)],

$$E_{\text{exo}} = E(\text{mol.}+2\text{H}) - E(\text{mol.}) - E(\text{IE-2H}), \quad (2)$$

while in the case of adsorption, E_{exo} is equivalent to the adsorption energy.

$$E_{\text{exo}} = E_{\text{ads}} = E(\text{mol.}+1\text{H}) - E(\text{mol.}) - E(1\text{H}). \quad (3)$$

E_{endo} has been calculated as the difference between the total energy of the interlayer-expanded 2H-$MoTe_2$ and 2H-$MoTe_2$,

$$E_{\text{endo}} = E(\text{IE-2H}) - E(2\text{H}). \quad (4)$$

The results show that the endothermic interlayer expansion is the dominant component of the intercalation energy for both NO_2+2H-$MoTe_2$ and N_2+2H-$MoTe_2$. In the case of NO_2, the effect is partially compensated by the exothermic molecule-sheet interactions (see Figure 5a), but for N_2, the intercalation energy is almost exclusively determined by the expansion (see Figure 5b). This is not just a product of the weak physisorption of N_2 but also the compression resulting from the sheet-sheet attraction. Without compression, the value of E_{exo} should be approximately equal to two exothermic adsorption energies for N_2+1H-$MoTe_2$ (-0.188 eV/nm^2), but the

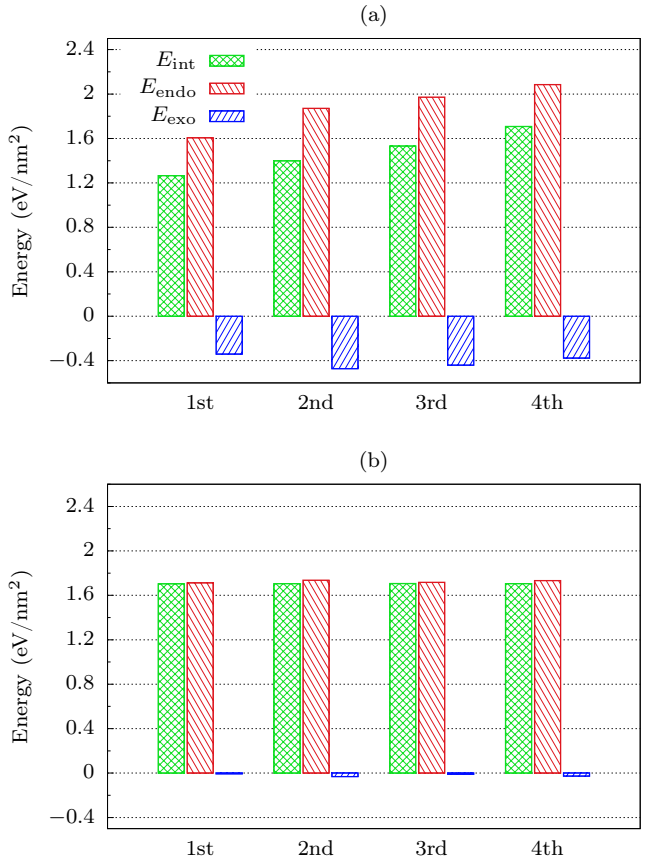

Figure 5: Intercalation energy and its endothermic and exothermic components shown for configurations of NO_2+2H-$MoTe_2$ (a) and N_2+2H-$MoTe_2$ (b).

molecule-sheet interactions for N_2+2H-$MoTe_2$ are notably weaker (≈ -0.02 eV/nm^2).

Compression effects also appear to be present in some structures of NO_2+2H-$MoTe_2$. The 1st configuration shows the lowest sheet expansion coupled with the weakest molecule-sheet interaction among NO_2+2H-$MoTe_2$, which is consistent with the effects of compression. This is further supported by the results for the 2nd and 3rd configurations, which have a significantly larger expansion and E_{exo} almost equal to $2E_{ads}$ for NO_2+1H-$MoTe_2$. On the other hand, the 4th configuration facilitates even greater expansion, but the molecule-sheet interaction becomes weaker. This suggests that the destabilization likely depends on the binding site and the molecule configuration, since these may result in different optimal distances between the molecule and the sheet.

As it has been shown, the intercalation energy differs between the configurations, but in all cases, its positive value has a common origin. The molecule-sheet interactions are not sufficient to compensate for the expansion. Thus, for the intercalation to be favorable, the expansion has to be reduced, and/or the molecule-sheet interaction has to be significantly stronger. As a consequence, the intercalation energy should depend on the concentration of the intercalated molecules, since the separation and the molecule-sheet binding energy per unit area will likely be affected by their coverage. Therefore, lower and higher concentrations could, in principle, result in lower intercalation energy and thus both should be tested.

1. Increased molecule concentration should increase the energy of the exothermic molecule-sheet interactions per unit area. Thus, it may help offset the endothermic interlayer expansion if the molecule-sheet binding is strong enough. The effect may compete with the increased expansion, but it may also reduce the compression, allowing effectively stronger molecular binding.

2. Reduced concentration of molecules should lower the endothermic expansion energy as the molecules will exert weaker repulsion per unit area. However, because of compression, this will likely reduce the energy of the molecule-sheet interactions. Hence, low concentrations should only be beneficial for species with strong binding.

3.5 Intercalation at different concentrations of molecules. Figure 6 shows how the intercalation energy changes depending on the molecule concentration. The initially-investigated structures have employed a 3×3 supercell, resulting in a concentration of 1.03 molecules/nm^2. Different concentrations have been achieved by adding molecules between sheets of $MoTe_2$ and/or expanding the supercell. Added molecules have been placed in the optimized structure of the previous coverage level in positions qualitatively equivalent to those of the lowest energy configuration shown in Figures 3a and 3b. Expanding the supercell was accomplished by increasing the lattice constant and adding the required atoms to the new cell (see Figures 1d–f). The expanded structures included 4×4 and 5×5 supercells.

First, let us consider the intercalation of NO_2+2H-$MoTe_2$-(3×3). Without the molecule, the intercalation energy is zero. As discussed in previous sections, one NO_2 gives an E_{int} of 1.265 eV/nm^2 and the coverage of 1.03 molecules/nm^2, making the intercalation unfavorable. However, adding molecules shows

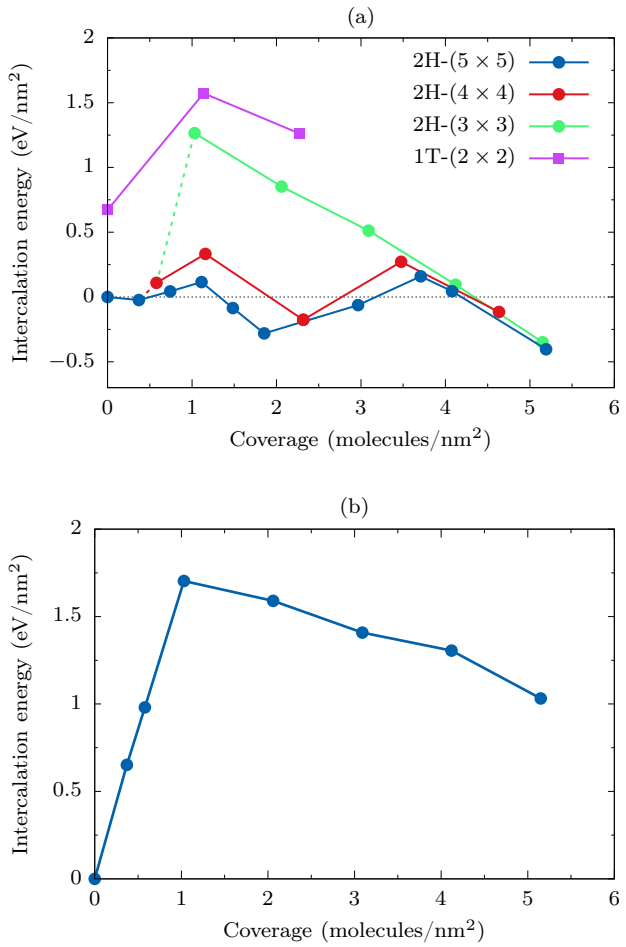

Figure 6: Intercalation energy at different levels of NO_2 (a) and N_2 (b) coverage.

the intercalation energy falling. It decreases approximately linearly, making the process energetically favorable above 4.3 molecules/nm^2. To elucidate the nature of this effect, the endo and exothermic components of the intercalation energy have been plotted in Figure 7a. The results show that the endothermic interlayer expansion energy increases with the coverage. However, the change is relatively low, illustrating that the subsequent molecules add little expansion. This allows the endothermic energy to remain lower than $2E(\text{1H-MoTe}_2) - E(\text{2H-MoTe}_2)$, which indicates that the intercalated sheets retain some of the original interlayer binding. Furthermore, despite the limited sheet expansion, the effect is still sufficient to reduce the compression of molecule-sheet interactions. Starting from $\approx$ 2 molecules/nm^2, the exothermic energy per molecule is almost equal to the energy of two NO_2 adsorptions on the surface of $MoTe_2$. Hence, the total exothermic energy becomes effectively a sum over molecule adsorptions on the upper and lower surfaces of $MoTe_2$, resulting in the linear increase of E_{exo}.

In contrast, the effects of intercalation in 4×4 and 5×5 supercells seem more complex in comparison. Figure 6a makes it apparent that the intercalation energies at comparable concentrations are notably lower when modeled in 4×4 and 5×5 supercells compared to 3×3 up until 3.5 molecules/nm^2. This indicates that for lower NO_2 coverage, the molecule-sheet interactions must be affected, which in turn should be reflected in the structure of the system. Figure 8 shows the optimized configurations of NO_2-intercalated 2H-$MoTe_2$-(5×5) (a,b) and 2H-$MoTe_2$-(4×4) (c–g) calculated at different levels of molecular coverage. In the case of 5×5, only selected structures are included, as they show qualitatively the same effects, but the size of the system and the number of the molecules at the interface make the relevant characteristics obfuscated.

Figures 8a–c illustrate the optimized configurations of NO_2+2H-$MoTe_2$ at coverages below 0.75 molecules/nm^2. The reduced molecule concentration

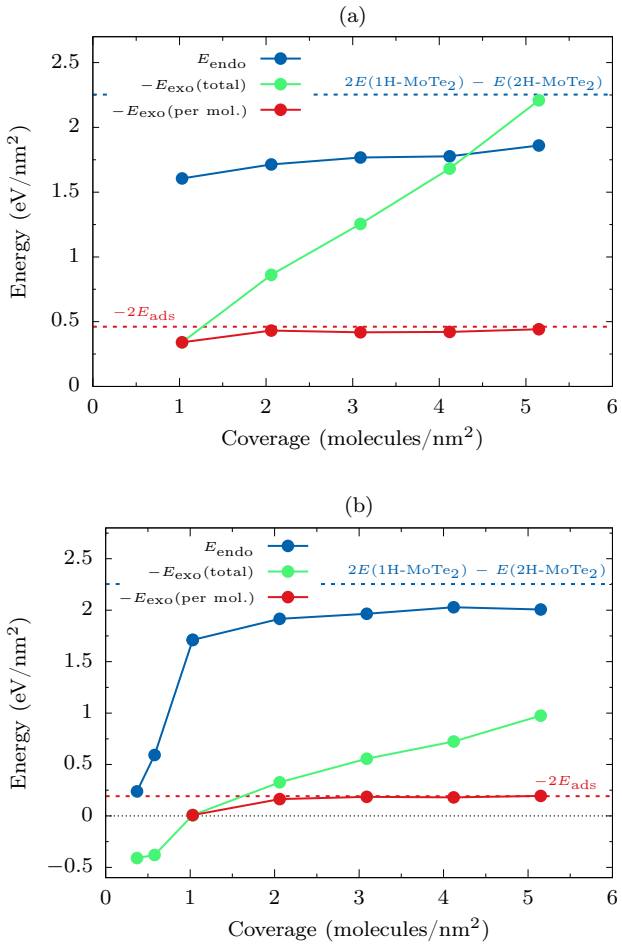

Figure 7: Endothermic and exothermic components of the intercalation energy of NO_2+2H-$MoTe_2$ (a) and N_2+2H-$MoTe_2$ (b).

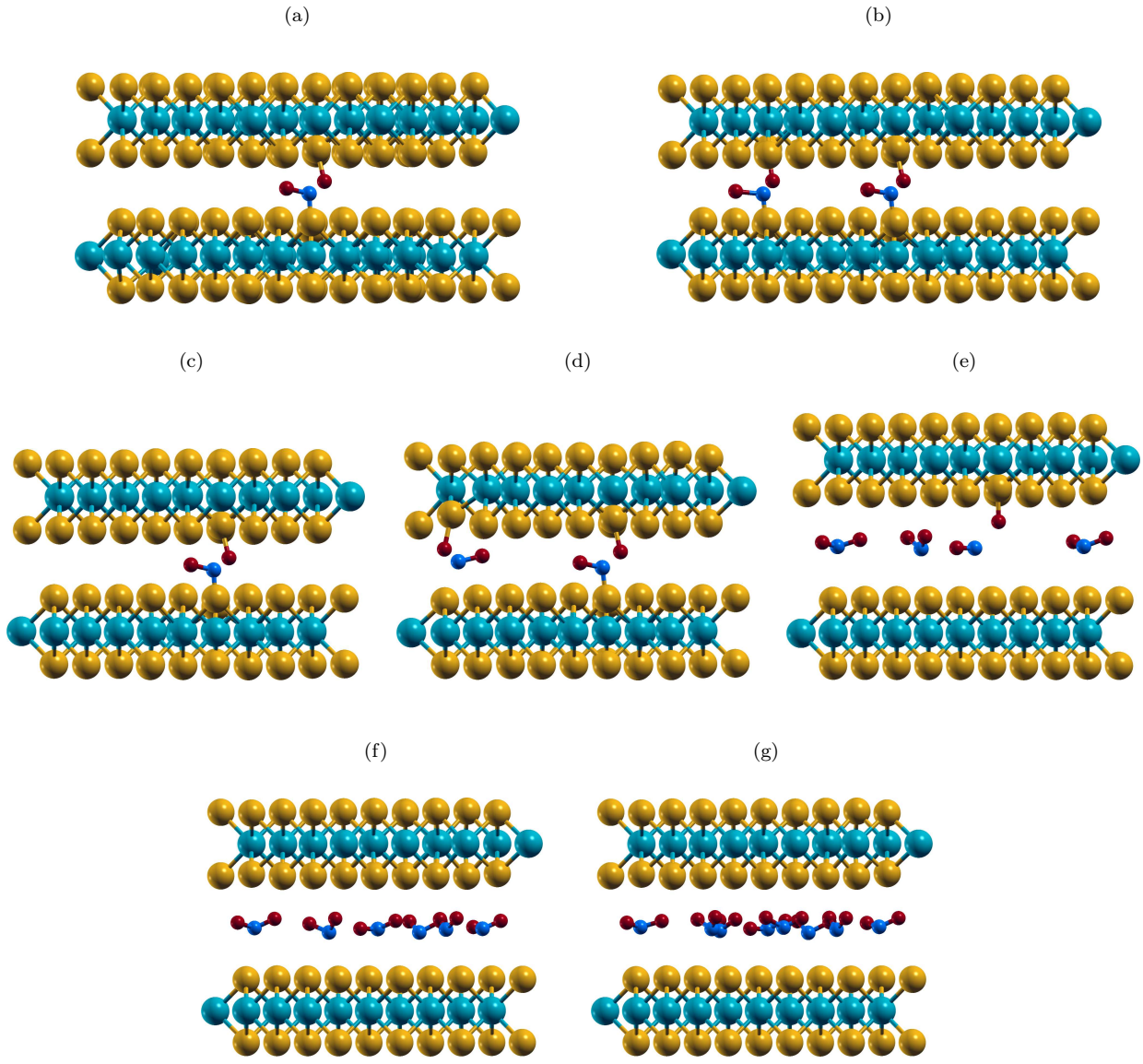

Figure 8: One (a) and two (b) molecules of NO_2 intercalated per 2H-$MoTe_2$-(5×5). One (c), two (d), four (e), six (f), and eight (g) molecules of NO_2 intercalated per 2H-$MoTe_2$-(4×4).

results in less endothermic expansion as the molecules exert weaker repulsion per unit area. Specifically, one molecule of NO_2 intercalated between the sheets of 2H-$MoTe_2$ in 4×4 and 5×5 cells (NO_2 coverage of 0.37 and 0.58 molecules/nm^2, Figures 8a and 8c) facilitates the expansion of 0.22 and 0.19 Å, respectively, while the 3×3 relaxation (1.03 molecules/nm^2) gives a much higher value of 2.11 Å. This illustrates that the contribution of the endothermic expansion to the total energy will be significantly reduced for low coverages of NO_2. However, this entails more than just a simple compression of the physisorptive interactions of NO_2. At low coverage, the interlayer binding overpowers the endothermic expansion, imposing sufficient force for the NO_2 molecules to dissociate into NO and O, which then can form strong chemical bonds with neighboring Te atoms. This significantly reduces the intercalation energy, making the process favorable at concentrations below 0.4 molecules/nm^2. Still, due to compression, the molecule-sheet interactions outside the new bond formation are endothermic. Hence, it is unlikely that E_{int} could get much lower than ≈ -25 meV/nm^2 while in the low coverage limit.

On the other hand, if the concentration continues to increase, the molecule-sheet repulsion per unit area will gradually get stronger. However, before overcoming the sheet binding, additional molecules will be able to dissociate. The results show that at ≈ 1.0 molecules/nm^2,

the interlayer binding is still sufficiently strong to split NO_2 if some molecules were previously dissociated (see Figure 8d). This allows a relatively low expansion of 0.52 Å and 0.47 Å obtained for 4×4 and 5×5 systems, respectively. In comparison, the 3×3 structures with comparable NO_2 coverage, but no dissociation, facilitate four times the expansion (2.1 Å, compare the optimized structures in Figures 8d and 3a). Consequently, the configurations with NO_2 dissociation facilitate lower E_{int} than those without it (0.335/0.115 vs. 1.265 eV/nm^2, see Figure 6a), but due to the increased interlayer separation, the intercalation at this concentration is energetically unfavorable in all cases. The small energy difference in the structures with NO_2 dissociation occurs, as in both cases some NO molecules decouple from the $MoTe_2$ surface. However, in the case of the 4×4 structure, it is one NO per two molecules, while in the 5×5 case, it is one per four, thus having a different impact on the interlayer expansion and consequently the energy.

Further increase in NO_2 coverage leads to molecule-sheet interactions overcoming the sheet binding, which entails a number of changes to the interface. The interlayer expansion grows (compare Figures 8d and 8e), which increases the endothermic component of intercalation. It also reduces the compression of the molecule-sheet interaction, which means that no additional molecules will dissociate. Instead, with the increased coverage, NO and O will gradually revert to NO_2 (see Figures 8c–f). It also means that the molecule-sheet interaction will contribute to the total energy via exothermic physisorption. Hence, before complete recombination, some NO_2 will remain dissociated with the products bonded to Te atoms, while others adopt an exothermic molecule-sheet interaction akin to that described in Section 3.4. In combination, it makes the intercalation energetically favorable between 1.5 and 3.0 molecules/nm^2, despite the large interlayer expansion. However, above 3.5 molecules/nm^2, all species recombine into NO_2. Hence, at high coverages, all systems behave qualitatively the same (see Figure 6a), with small differences in E_{int} facilitated by variation in molecule configurations and sheet alignment (larger cells show a lower lateral shift).

Consequently, there are three coverage ranges where intercalation can be favorable: low ($<$ 0.4 molecules/nm^2), mid (1.5 to 3.0 molecules/nm^2), and high ($>$ 4.0 molecules/nm^2). Those are separated by two energy barriers at $\approx$ 1.0 and $\approx$ 3.5 molecules/nm^2. The first energy barrier is relatively low and asymmetric. Hence, pockets of mixed species will likely be formed and grow with the increased concentration, while low coverage areas will facilitate easier intercalation of new molecules. Similarly, the second barrier suggests that high coverage will exhibit growing pockets of fully recombined higher-concentration NO_2 rather than uniform increases in coverage.

It is prudent to note that limited-scope tests have been made for NO_2+1T-$MoTe_2$-(2×2). The molecules have been oriented on Mo-Te bridge positions similar to that of the 1st configuration of NO_2+2H-$MoTe_2$. The results have shown that the system has the highest intercalation energy among the investigated structures (despite NO_2 dissociation), which makes a 2H-to-1T phase transition unlikely. Further probing of the interface could, in principle, find lower energy configurations. However, a sufficiently large shift seems doubtful, especially since molecule-sheet interactions tend to favor the 2H phase[57].

In contrast, N_2 intercalation is a notably less complex process. There is no dissociation in the low-coverage limit. Therefore, due to the dominance of the sheet binding, the intercalation has no exothermic component. Rather, the intercalation energy comprises the endothermic sheet expansion and the endothermic molecule-sheet repulsion (see Figure 7b). Thus, the intercalation is not favorable, reaching its maximum value at 1.03 molecules/nm^2. At higher coverages the molecule-sheet interactions become exothermic, which helps lower the energy. However, since N_2 interacts weaker and facilitates higher expansion than NO_2, the effect is relatively slow (see Figure 6b). Even at a coverage of 5.15 molecules/nm^2, the intercalation energy is still far from favorable, owing to a notable difference between endothermic expansion and exothermic molecule-sheet interactions (Figure 7b). Consequently, N_2 intercalation is unlikely to be energetically favorable before decoupling the sheets, which shows that intercalation between sheets of $MoTe_2$ is a selective process favoring reactive species.

3.6 Intercalation and its impact on sensing. As it has been shown, the interactions between NO_2 and $MoTe_2$ can be quite complex. Hence, it is prudent to consider the stages of intercalation and evacuation as they pertain to the operations of a 2H-$MoTe_2$ sensor. If exposed to a NO_2 environment, the molecules should be able to intercalate between sheets of $MoTe_2$ as the process is energetically favorable. The resulting equilibrium coverage (equal rates of intercalation and evac-

uation) would then depend on the NO_2 reservoir. Thus, to accommodate different possibilities, the analysis will span from low to high coverages.

When first NO_2 molecules intercalate, the molecule-sheet interactions are too weak to overcome the interlayer binding and facilitate sufficient interlayer expansion. Therefore, to accommodate the low expansion, the molecules dissociate, and the NO and O species bond to Te atoms, resulting in a charge accumulation of -1.158 and -0.687 e, respectively. This significantly enhances the per molecule response (-1.844 e) relative to the intercalation without dissociation (-0.363 e) or adsorption (-0.166 e). Thus, the dissociation should not only notably reduce the intercalation energy but also improve the sensitivity of a multilayer system. This is especially true for low concentrations of NO_2 since all molecules split. Still, mid coverages also benefit as the interface comprises a mix of NO_2, NO, and O species. Hence, depending on the ratio, the average transfer will range between -1.844 and ≈ -0.4 e. On the other hand, at high coverages, all molecules recombine. However, the average charge transfer per NO_2 (-0.363 e) is more than twice that of the adsorption (-0.166 e). Hence, in all cases, intercalation should notably improve the sensitivity of 2H-$MoTe_2$.

If NO_2 evacuates from the environment, it will also begin to evacuate from the intercalated 2H-$MoTe_2$. When in the high-coverage limit, loss of NO_2 would increase the intercalation energy. Subsequently, moving below 4.0 molecules/nm^2 would make the intercalation unfavorable, which in turn would accelerate the evacuation. Furthermore, the process would not immediately facilitate NO_2 dissociation, as it requires low NO_2 coverage to occur. Rather, the system would continue to favor the quick removal of NO_2 following the increase of intercalation energy along the path of the 2H-$MoTe_2$-(3×3), and only below 1.0 molecules/nm^2, dissociation would begin. This would slow down the process. However, as the intercalation energy in the low-coverage limit is only ≈ -25 meV/nm^2, the process should continue, allowing 2H-$MoTe_2$ recovery.

4 Conclusions

The present work demonstrates a computational investigation of the intercalation of NO_2 and N_2 between sheets of 2H-$MoTe_2$. The results show that the intercalation of NO_2 can be energetically favorable depending on the molecule coverage of the interface. First, < 0.4, then between 1.5 and 3.0, and finally > 4.0 molecules/nm^2. In the first case, the molecule-sheet interactions are too weak to overcome the interlayer binding and facilitate sufficient interlayer expansion. Thus, to accommodate the low separation, the molecules dissociate, and the NO and O species bond to the Te atoms. In the second case, the molecule-sheet interactions are sufficiently strong to facilitate a larger interlayer expansion. This enables some of the species to recombine back into NO_2. However, the interface still comprises a mix of NO_2, NO, and O species. Finally, the third case has all species recombined back into NO_2, and the intercalation energy is dominated by the physisorptive interactions between molecules and sheets. On the other hand, the results also show that the intercalation is unlikely to facilitate the 2H-to-1T transition of $MoTe_2$.

The dissociation and non-dissociative intercalation of NO_2 enhance the per molecule charge transfer by 1110% and 256%, respectively, relative to adsorption on the surface. Hence, in all favorable cases, the intercalation should significantly enhance the response of the system. Furthermore, the results suggest that the evacuation of NO_2 should be feasible, allowing efficient 2H-$MoTe_2$ recovery. Consequently, the findings show that the reported enhancement of the sensitivity of multilayer TMDs could be facilitated by intercalation. The results also show that the intercalation between sheets of 2H-$MoTe_2$ can be quite selective, as N_2 intercalation will likely not be favorable regardless of the coverage. It suggests that non-interactive stable molecules are less likely to intercalate between the sheets, which could explain why the reported enhancement for multilayer TMDs varied between analytes.

Acknowledgement This work was supported by the Ministry of Science and Higher Education in Poland (Grant No. 0512/SBAD/2120) within the project realized at the Institute of Physics, Poznan University of Technology. Calculations reported in this work have been performed at the Interdisciplinary Center for Mathematical and Computational Modeling (ICM) of the University of Warsaw under Grant No. GB81-3.

References

(1) Xu, H.; Zhang, H.; Guo, Z.; Shan, Y.; Wu, S.; Wang, J.; Hu, W.; Liu, H.; Sun, Z.; Luo, C. et al. High-Performance Wafer-Scale MoS_2 Transistors toward Practical Application. *Small* **2018**, *14*, 1803465.

(2) Wu, E.; Xie, Y.; Yuan, B.; Zhang, H.; Hu, X.; Liu, J.; Zhang, D.

Ultrasensitive and Fully Reversible NO_2 Gas Sensing Based on p-Type $MoTe_2$ under Ultraviolet Illumination. *ACS Sensors* **2018**, *3*, 1719–1726.

(3) Li, G.; Huang, B.; Pan, Z.; Su, X.; Shao, Z.; An, L. Advances in three-dimensional graphene-based materials: configurations, preparation and application in secondary metal (Li, Na, K, Mg, Al)-ion batteries. *Energy Environ. Sci.* **2019**, *12*, 2030–2053.

(4) Askari, M. B.; Beheshti-Marnani, A.; Seifi, M.; Rozati, S. M.; Salarizadeh, P. Fe_3O_4@MoS_2/RGO as an effective nano-electrocatalyst toward electrochemical hydrogen evolution reaction and methanol oxidation in two settings for fuel cell application. *Journal of Colloid and Interface Science* **2019**, *537*, 186–196.

(5) Qiao, J.; Wang, S.; Wang, Z.; He, C.; Zhao, S.; Xiong, X.; Wang, S.; Zhang, X.; Tao, X. Ultrasensitive and Broadband All-Optically Controlled THz Modulator Based on $MoTe_2$/Si van der Waals Heterostructure. *Advanced Optical Materials* **2020**, *8*, 2000160.

(6) El-Ahmar, S.; Szary, M. J.; Ciuk, T.; Prokopowicz, R.; Dobrowolski, A.; Jagiełło, J.; Ziemba, M. Graphene on SiC as a promising platform for magnetic field detection under neutron irradiation. *Applied Surface Science* **2022**, *590*, 152992.

(7) Bhandavat, R.; David, L.; Singh, G. Synthesis of Surface-Functionalized WS_2 Nanosheets and Performance as Li-Ion Battery Anodes. *The Journal of Physical Chemistry Letters* **2012**, *3*, 1523–1530.

(8) Shao, X.; Wang, K.; Pang, R.; Shi, X. Lithium Intercalation in Graphene/MoS_2 Composites: First-Principles Insights. *The Journal of Physical Chemistry C* **2015**, *119*, 25860–25867.

(9) Liu, Y.; Zhang, N.; Kang, H.; Shang, M.; Jiao, L.; Chen, J. WS_2 Nanowires as a High-Performance Anode for Sodium-Ion Batteries. *Chemistry – A European Journal* **2015**, *21*, 11878–11884.

(10) Ren, X.; Zhao, Q.; McCulloch, W. D.; Wu, Y. MoS_2 as a long-life host material for potassium ion intercalation. *Nano Research* **2017**, *10*, 1313–1321.

(11) Larson, D. T.; Fampiou, I.; Kim, G.; Kaxiras, E. Lithium Intercalation in Graphene–MoS_2 Heterostructures. *The Journal of Physical Chemistry C* **2018**, *122*, 24535–24541.

(12) Sheng, J.; Wang, T.; Tan, J.; Lv, W.; Qiu, L.; Zhang, Q.; Zhou, G.; Cheng, H.-M. Intercalation-Induced Conversion Reactions Give High-Capacity Potassium Storage. *ACS Nano* **2020**, *14*, 14026–14035.

(13) Panda, M. R.; Gangwar, R.; Muthuraj, D.; Sau, S.; Pandey, D.; Banerjee, A.; Chakrabarti, A.; Sagdeo, A.; Weyland, M.; Majumder, M. et al. High Performance Lithium-Ion Batteries Using Layered 2H-$MoTe_2$ as Anode. *Small* **2020**, *16*, 2002669.

(14) Panda, M. R.; Sau, S.; Bao, Q.; Majumder, M.; Mitra, S. Layered 2H$MoTe_2$: A novel anode material for lithium-ion batteries. *Materials Today: Proceedings* **2022**, *50*, 113–116, International Virtual Conference on Advanced Nanomaterials and Applications (VCAN).

(15) Zhou, R.; Wang, H.; Chang, J.; Yu, C.; Dai, H.; Chen, Q.; Zhou, J.; Yu, H.; Sun, G.; Huang, W. Ammonium Intercalation Induced Expanded 1T-Rich Molybdenum Diselenides for Improved Lithium Ion Storage. *ACS Applied Materials & Interfaces* **2021**, *13*, 17459–17466.

(16) Dai, H.; Tang, M.; Huang, J.; Wang, Z. A Series of Molecule-Intercalated MoS_2 as Anode Materials for Sodium Ion Batteries. *ACS Applied Materials & Interfaces* **2021**, *13*, 10870–10877.

(17) Liu, H.; Wang, J.-G.; Hua, W.; You, Z.; Hou, Z.; Yang, J.; Wei, C.; Kang, F. Boosting zinc-ion intercalation in hydrated MoS_2 nanosheets toward substantially improved performance. *Energy Storage Materials* **2021**, *35*, 731–738.

(18) Huang, M.; Mai, Y.; Zhao, L.; Liang, X.; Fang, Z.; Jie, X. Tuning the kinetics of zinc ion in MoS_2 by polyaniline intercalation. *Electrochimica Acta* **2021**, *388*, 138624.

(19) Xie, J.; Zhang, J.; Li, S.; Grote, F.; Zhang, X.; Zhang, H.; Wang, R.; Lei, Y.; Pan, B.; Xie, Y. Controllable Disorder Engineering in Oxygen-Incorporated MoS_2 Ultrathin Nanosheets for Efficient Hydrogen Evolution. *Journal of the American Chemical Society* **2013**, *135*, 17881–17888.

(20) Wu, Z.; Tang, C.; Zhou, P.; Liu, Z.; Xu, Y.; Wang, D.; Fang, B. Enhanced hydrogen evolution catalysis from osmotically swollen ammoniated MoS_2. *J. Mater. Chem. A* **2015**, *3*, 13050–13056.

(21) Palencia-Ruiz, S.; Uzio, D.; Legens, C.; Laurenti, D.; Afanasiev, P. Stability and catalytic properties of 1T-MoS_2 obtained via solvothermal synthesis. *Applied Catalysis A: General* **2021**, *626*, 118355.

(22) Levita, G.; Righi, M. C. Effects of Water Intercalation and Tribochemistry on MoS_2 Lubricity: An Ab Initio Molecular Dynamics Investigation. *ChemPhysChem* **2017**, *18*, 1475–1480.

(23) Yang, Z.; Bhowmick, S.; Sen, F. G.; Alpas, A. T. Microscopic and atomistic mechanisms of sliding friction of MoS_2: Effects of undissociated and dissociated H_2O. *Applied Surface Science* **2021**, *563*, 150270.

(24) Bermudez, V. M. Computational Study of the Adsorption of NO_2: on Monolayer MoS_2. *The Journal of Physical Chemistry C* **2020**, *124*, 15275–15284.

(25) Deng, X.; Liang, X.; Ng, S.-P.; Wu, C.-M. L. Adsorption of formaldehyde on transition metal doped monolayer MoS_2: A DFT study. *Applied Surface Science* **2019**, *484*, 1244–1252.

(26) Panigrahi, P.; Hussain, T.; Karton, A.; Ahuja, R. Elemental Substitution of Two-Dimensional Transition Metal Dichalcogenides ($MoSe_2$ and $MoTe_2$): Implications for Enhanced Gas Sensing. *ACS Sensors* **2019**, *4*, 2646–2653, PMID: 31565924.

(27) Szary, M. J.; Florjan, D. M.; Bąbelek, J. A. Selective Detection of Carbon Monoxide on P-Block Doped Monolayers of $MoTe_2$. *ACS Sensors* **2022**, *7*, 272–285, PMID: 35044171.

(28) Pham, T.; Li, G.; Bekyarova, E.; Itkis, M. E.; Mulchandani, A. MoS_2-Based Optoelectronic Gas Sensor with Sub-parts-per-billion Limit of NO_2 Gas Detection. *ACS Nano* **2019**, *13*, 3196–3205.

(29) Donarelli, M.; Prezioso, S.; Perrozzi, F.; Bisti, F.; Nardone, M.; Giancaterini, L.; Cantalini, C.; Ottaviano, L. Response to NO_2 and other gases of resistive chemically exfoliated MoS_2-based gas sensors. *Sensors and Actuators B: Chemical* **2015**, *207*, 602–613.

(30) Shackery, I.; Pezeshki, A.; Park, J. Y.; Palanivel, U.; Kwon, H. J.; Yoon, H. S.; Im, S.; Cho, J. S.; Jun, S. C. Few-layered α-$MoTe_2$ Schottky junction for a high sensitivity chemical-vapour sensor. *J. Mater. Chem. C* **2018**, *6*, 10714–10722.

(31) Sharma, S.; Kumar, A.; Kaur, D. Room temperature ammonia gas sensing properties of MoS_2 nanostructured thin film. *AIP Conference Proceedings* **2018**, *1953*.

(32) Feng, Z.; Xie, Y.; Wu, E.; Yu, Y.; Zheng, S.; Zhang, R.; Chen, X.; Sun, C.; Zhang, H.; Pang, W. et al. Enhanced Sensitivity of $MoTe_2$ Chemical Sensor through Light Illumination. *Micromachines* **2017**, *8*.

(33) Järvinen, T.; Lorite, G. S.; Peräntie, J.; Toth, G.; Saarakkala, S.; Virtanen, V. K.; Kordas, K. WS_2 and MoS_2 thin film gas sensors with high response to NH_3 in air at low temperature. *Nanotechnology* **2019**, *30*, 405501.

(34) Late, D. J.; Huang, Y.-K.; Liu, B.; Acharya, J.; Shirodkar, S. N.; Luo, J.; Yan, A.; Charles, D.; Waghmare, U. V.; Dravid, V. P. et al. Sensing Behavior of Atomically Thin-Layered MoS_2 Transistors. *ACS Nano* **2013**, *7*, 4879–4891, PMID: 23713986.

(35) Jin, W.; Yeh, P.-C.; Zaki, N.; Zhang, D.; Sadowski, J. T.; Al-Mahboob, A.; van der Zande, A. M.; Chenet, D. A.; Dadap, J. I.; Herman, I. P. et al. Direct Measurement of the Thickness-Dependent Electronic Band Structure of MoS_2 Using Angle-Resolved Photoemission Spectroscopy. *Phys. Rev. Lett.* **2013**, *111*, 106801.

(36) Andersen, M.; Hornekær, L.; Hammer, B. Understanding intercalation structures formed under graphene on Ir(111). *Phys. Rev. B* **2014**, *90*, 155428.

(37) Cook, B.; Russakoff, A.; Varga, K. Coverage dependent work function of graphene on a Cu(111) substrate with intercalated alkali metals. *Applied Physics Letters* **2015**, *106*, 211601.

(38) Pervan, P.; Lazić, P. Adsorbed or intercalated: Na on graphene/Ir(111). *Phys. Rev. Materials* **2017**, *1*, 044202.

(39) Perilli, D.; Fiori, S.; Panighel, M.; Liu, H.; Cepek, C.; Peressi, M.; Comelli, G.; Africh, C.; Di Valentin, C. Mechanism of CO Intercalation through the Graphene/Ni(111) Interface and Effect of Doping. *The Journal of Physical Chemistry Letters* **2020**, *11*, 8887–8892.

(40) Xu, J.; Zhang, J.; Zhang, W.; Lee, C.-S. Interlayer Nanoarchitectonics of Two-Dimensional Transition-Metal Dichalcogenides Nanosheets for Energy Storage and Conversion Applications. *Advanced Energy Materials* **2017**, *7*, 1700571.

(41) Rasamani, K. D.; Alimohammadi, F.; Sun, Y. Interlayer-expanded MoS_2. *Materials Today* **2017**, *20*, 83–91.

(42) Yousaf, M.; Wang, Y.; Chen, Y.; Wang, Z.; Firdous, A.; Ali, Z.; Mahmood, N.; Zou, R.; Guo, S.; Han, R. P. S. A 3D Trilayered CNT/$MoSe_2$/C Heterostructure with an Expanded $MoSe_2$ Interlayer Spacing for an Efficient Sodium Storage. *Advanced Energy Materials* **2019**, *9*, 1900567.

(43) Kozawa, D.; Kumar, R.; Carvalho, A.; Kumar Amara, K.; Zhao, W.; Wang, S.; Toh, M.; Ribeiro, R. M.; Castro Neto, A. H.; Matsuda, K. et al. Photocarrier relaxation pathway in two-dimensional semiconducting transition metal dichalcogenides. *Nature Communications* **2014**, *5*, 4543.

(44) Ko, B. M.; Khan, M. F.; Dastgeer, G.; Han, G. N.; Khan, M. A.; Eom, J. Reconfigurable carrier type and photodetection of $MoTe_2$ of various thicknesses by deep ultraviolet light illumination. *Nanoscale Adv.* **2022**, *4*, 2744–2751.

(45) Giannozzi, P.; Baroni, S.; Bonini, N.; Calandra, M.; Car, R.; Cavazzoni, C.; Ceresoli, D.; Chiarotti, G. L.; Cococcioni, M.; Dabo, I. et al. QUANTUM ESPRESSO: a modular and open-source software project for quantum simulations of materials. *Journal of Physics: Condensed Matter* **2009**, *21*, 395502.

(46) Giannozzi, P.; Andreussi, O.; Brumme, T.; Bunau, O.; Nardelli, M. B.; Calandra, M.; Car, R.; Cavazzoni, C.; Ceresoli, D.; Cococcioni, M. et al. Advanced capabilities for materials modelling with QUANTUM ESPRESSO. *Journal of Physics: Condensed Matter* **2017**, *29*, 465901.

(47) Giannozzi, P.; Baseggio, O.; Bonfà, P.; Brunato, D.; Car, R.; Carnimeo, I.; Cavazzoni, C.; de Gironcoli, S.; Delugas, P.; Ferrari Ruffino, F. et al. Quantum ESPRESSO toward the exascale. *The Journal of Chemical Physics* **2020**, *152*, 154105.

(48) Kokalj, A. XCrySDen—a new program for displaying crystalline structures and electron densities. *Journal of Molecular Graphics and Modelling* **1999**, *17*, 176–179.

(49) Perdew, J. P.; Ruzsinszky, A.; Csonka, G. I.; Vydrov, O. A.; Scuseria, G. E.; Constantin, L. A.; Zhou, X.; Burke, K. Restoring the Density-Gradient Expansion for Exchange in Solids and Surfaces. *Phys. Rev. Lett.* **2008**, *100*, 136406.

(50) Perdew, J. P.; Burke, K.; Ernzerhof, M. Generalized Gradient Approximation Made Simple. *Phys. Rev. Lett.* **1996**, *77*, 3865–3868.

(51) Vanderbilt, D. Soft self-consistent pseudopotentials in a generalized eigenvalue formalism. *Phys. Rev. B* **1990**, *41*, 7892–7895.

(52) Rappe, A. M.; Rabe, K. M.; Kaxiras, E.; Joannopoulos, J. D. Optimized pseudopotentials. *Phys. Rev. B* **1990**, *41*, 1227–1230.

(53) Grimme, S.; Antony, J.; Ehrlich, S.; Krieg, H. A consistent and accurate ab initio parametrization of density functional dispersion correction (DFT-D) for the 94 elements H-Pu. *The Journal of Chemical Physics* **2010**, *132*, 154104.

(54) Shuai, J.; Yoo, H. D.; Liang, Y.; Li, Y.; Yao, Y.; Grabow, L. C. Density functional theory study of Li, Na, and Mg intercalation and diffusion in MoS_2 with controlled interlayer spacing. *Materials Research Express* **2016**, *3*, 064001.

(55) Liang, H.; Cao, Z.; Ming, F.; Zhang, W.; Anjum, D. H.; Cui, Y.; Cavallo, L.; Alshareef, H. N. Aqueous Zinc-Ion Storage in MoS_2 by Tuning the Intercalation Energy. *Nano Letters* **2019**, *19*, 3199–3206, PMID: 30986352.

(56) Massaro, A.; Pecoraro, A.; Muñoz-García, A. B.; Pavone, M. First-Principles Study of Na Intercalation and Diffusion Mechanisms at 2D MoS_2/Graphene Interfaces. *The Journal of Physical Chemistry C* **2021**, *125*, 2276–2286, PMID: 33584936.

(57) Zhou, Y.; Reed, E. J. Structural Phase Stability Control of Monolayer $MoTe_2$ with Adsorbed Atoms and Molecules. *The Journal of Physical Chemistry C* **2015**, *119*, 21674–21680.

TOC Graphic